Kolmogorov-Hinze Scales in Turbulent Superfluids

Tsuyoshi Kadokura and Hiroki Saito
Department of Engineering Science, University of Electro-Communications, Tokyo 182-8585, Japan

(Received 29 July 2023; accepted 18 November 2024; published 16 December 2024)

When a two-component mixture of immiscible fluids is stirred, the fluids are split into smaller domains with more vigorous stirring. We numerically investigate the sizes of such domains in a fully developed turbulent state of a two-component superfluid stirred with energy input rate ϵ. For the strongly immiscible condition, the typical domain size is shown to be proportional to $\epsilon^{-2/5}$, as predicted by the Kolmogorov-Hinze theory in classical fluids. For the weakly immiscible condition, quantum effects become pronounced and the power changes from $-2/5$ to $-1/4$.

DOI: 10.1103/PhysRevLett.133.256001

When oil is poured into water and these fluids are stirred, the oil becomes split into droplets in the water. The droplet sizes become smaller with more vigorous stirring. Such disintegration phenomena in multicomponent fluids are ubiquitous in nature, and are important in engineering and industry.

Kolmogorov [1] and Hinze [2] considered the disintegration process of droplets, and estimated the size of droplets in turbulent fluids. In fully developed turbulence, the energy is input into the system as large-scale eddies, which cascades toward a smaller scale, resulting in the Kolmogorov power law of the energy spectrum [3]. In such turbulent fluids, large-size droplets are unstable because they are susceptible to deformation and disintegration due to the fluctuating pressure of the surrounding fluid. Small droplets are thus produced by the breakup of large droplets, and this breakup process continues to a scale where the turbulent energy to break up the droplets becomes balanced with the droplet energy that sustains their shape. Droplets smaller than this scale coalesce into large droplets. Therefore, there exists a characteristic size D for droplets in turbulent fluids, which is referred to as the Kolmogorov-Hinze (KH) scale, given by [2]

$$D \sim (\sigma/\rho)^{3/5}\epsilon^{-2/5}, \tag{1}$$

where σ is the interfacial tension coefficient, ρ is the density of the surrounding fluid, and ϵ is the energy input rate to maintain the turbulence. The KH scale has been experimentally verified in various systems [4–8]. Furthermore, direct numerical simulations have been performed over the last decade [9–15].

In this Letter, we extend the study of KH scales to a quantum mechanical system: the superfluid turbulence of a two-component Bose-Einstein condensate (BEC). We will show that the KH scale also appears in superfluids and is modified by quantum effects. Turbulent behavior in superfluids has been widely studied. For single-component superfluids, a steady or decaying turbulent state exhibits the Kolmogorov power law [16–31]. The turbulent behavior of gaseous BECs has also been experimentally studied [32–34], and a power law behavior has been observed recently [35–40]. A wide variety of systems have been studied theoretically, such as two-dimensional systems [41–48], dipolar superfluids [49], and boundary layers [50]. Here, we focus on the turbulence in a two-component BEC. Turbulence in multicomponent BECs has been investigated by many researchers [51–64]. In the context of domain-size scaling in multicomponent BECs, coarsening dynamics following domain formation have been studied extensively [65–79]. However, the KH scale, i.e., domain-size scaling in conjunction with Kolmogorov turbulence, has not yet been investigated.

The power law of the KH scale in Eq. (1) can be derived as follows. The typical domain size is determined by the competition between the two energies,

$$E_{\mathrm{breakup}} \sim E_{\mathrm{coalesce}}, \tag{2}$$

where E_{breakup} and E_{coalesce} are the energies relevant to breakup and coalescence of domains, respectively. For a length scale ℓ, E_{breakup} may be given by the kinetic energy $\sim\rho\ell^3 v^2$, where v is the typical velocity on the length scale ℓ. Within the inertial range of the Kolmogorov turbulence, v obeys the two-thirds law [3], $v^2 \sim (\epsilon\ell)^{2/3}$, and hence, $E_{\mathrm{breakup}} \sim \rho\epsilon^{2/3}\ell^{11/3}$. On the other hand, if the interfacial tension plays a crucial role in the coalescence process, E_{coalesce} is given by $\sim\sigma\ell^2$. Although the KH scale D is not expected to be in the inertial range [11], we extrapolate E_{breakup} based on the two-thirds law to the scale where E_{coalesce} is dominant. Equation (2) then gives the typical length scale ℓ, which corresponds to the KH scale D in Eq. (2). The KH scale also follows from a simple dimensional analysis, assuming that D is determined only by ρ, σ, and ϵ.

The interfacial tension is well defined also for a phase-separated two-component BEC [80–82]. Therefore, we expect that the KH scale in Eq. (1) also emerges in two-component BECs, when the domain size D is much larger than the interface thickness. In the phase-separated BEC, the competition between the quantum pressure and the intercomponent repulsion gives a characteristic length scale W [see Eq. (5)]. When $D \gg W$, W can be interpreted as the interface thickness and the KH scale in Eq. (1) will hold. However, for $D \ll W$, the picture of the interfacial tension breaks down in the derivation of Eq. (1). In this regime, the quantum pressure plays a dominant role in the coalescence of domains, and E_{coalesce} is given by the quantum kinetic energy (per domain), $\sim nD^3\hbar^2/(mD^2)$, where n and m are the atomic number density and mass, respectively. In this case, Eq. (2) gives the characteristic size as

$$D \sim (\hbar/m)^{3/4}\epsilon^{-1/4}. \tag{3}$$

Therefore, in the limit of weak segregation with large W, the quantum mechanical effect becomes pronounced and the KH scale is expected to change from the $-2/5$ to $-1/4$ power law with respect to ϵ. In the remainder of this Letter, we will corroborate this prediction using numerical simulations of the coupled Gross-Pitaevskii (GP) equations.

In the mean-field approximation, a two-component BEC at zero temperature is described by the coupled GP equations,

$$i\hbar\frac{\partial\psi_1}{\partial t} = \left(-\frac{\hbar^2}{2m}\nabla^2 + V_{\mathrm{ext}} + g_{11}|\psi_1|^2 + g_{12}|\psi_2|^2\right)\psi_1, \tag{4a}$$

$$i\hbar\frac{\partial\psi_2}{\partial t} = \left(-\frac{\hbar^2}{2m}\nabla^2 + V_{\mathrm{ext}} + g_{22}|\psi_2|^2 + g_{12}|\psi_1|^2\right)\psi_2, \tag{4b}$$

where $\psi_j(\boldsymbol{r}, t)$ is the macroscopic wave function for the jth component, $V_{\mathrm{ext}}(\boldsymbol{r}, t)$ is the external stirring potential, and $g_{jj'} = 4\pi\hbar^2 a_{jj'}/m$ with $a_{jj'}$ being the s-wave scattering length between the jth and j'th components.

The miscibility between the two components is determined by the coupling coefficients $g_{jj'}$. The two superfluids are immiscible and phase separation occurs when $g_{12}^2 > g_{11}g_{22}$ is satisfied [83]. In the following, for simplicity, we assume $g_{11} = g_{22} \equiv g > 0$ and $g_{12} > 0$; therefore, the immiscible condition reduces to $g_{12} > g$. We also assume $g_{12}/g - 1 \ll 1$. The characteristic length scale in the phase separation, over which the density of each component changes from 0 to n (or n to 0) in an infinite system, has the form [80–82]

$$W \simeq \xi(g_{12}/g - 1)^{-1/2}, \tag{5}$$

where $\xi \equiv \hbar/(mgn)^{1/2}$ is the healing length. When W is much smaller than the domain size D, W corresponds to the interface thickness of domains. In this case, the interfacial tension coefficient is given by [80–82]

$$\sigma \simeq \left[\frac{\hbar^2 n^3}{2m}(g_{12} - g)\right]^{1/2}. \tag{6}$$

In the following, the length, time, and wave functions are normalized by W, $mW^2/\hbar$, and $\sqrt{n}$, respectively, where n is the average density of each component. In this unit, the normalized interaction coefficients, $\tilde{g}$ and $\tilde{g}_{12}$, in the GP equation become (see Supplemental Material [84] for details)

$$\tilde{g} = \frac{g}{g_{12} - g}, \tag{7}$$

and $\tilde{g}_{12} = g_{12}/(g_{12} - g) = \tilde{g} + 1$; therefore, the interaction coefficients are reduced to the single parameter $\tilde{g}$. The GP equation is numerically solved using the split-step Fourier method [85], and the periodic boundary condition is imposed. The numerical box with size $L^3 = (512\tilde{\xi})^3$ is discretized into a 512^3 mesh, where the nondimensional healing length is $\tilde{\xi} \equiv \xi/W = 1/\sqrt{\tilde{g}}$. The two components are equally populated, $\int|\psi_1|^2 d\boldsymbol{r} = \int|\psi_2|^2 d\boldsymbol{r} = L^3$, and the initial state has a uniform density with random phases on each mesh.

To input the large-scale turbulent energy, the system is stirred using plate-shaped potentials given by

$$V_{\mathrm{ext}}(\boldsymbol{r}, t) = V_0 \sum_{\{X,Y\}} e^{-\left[X - \frac{L}{2}\sin(\Omega t + \phi_{XY})\right]^2}\theta(L/4 - |Y|), \tag{8}$$

where the potential height is taken to be $V_0 = 2$, θ is the Heaviside step function, and the summation is taken over $\{X, Y\} = \{x, y\}$, $\{y, z\}$, and $\{z, x\}$ with $\phi_{XY} = 0$, $2\pi/3$, and $4\pi/3$, respectively. The three plate-shaped potentials oscillating in the x, y, and z directions produce isotropic turbulence. (See the movie in the Supplemental Material [84] showing how the plate-shaped potentials stir the system.) The maximum Mach number of the plate-shaped potentials in the sinusoidal motion is defined as

$$M \equiv \frac{\Omega L}{2v_s}, \tag{9}$$

where $v_s = \sqrt{2\tilde{g}}$ is the sound velocity.

To realize a steady turbulent state, the energy must be dissipated on a small length scale. For this purpose, the term $-\gamma(\nabla \cdot \boldsymbol{J})\psi_j$ is added to the right-hand sides of Eq. (4) (see Supplemental Material for detail [84]), where γ is a positive constant and

$$\boldsymbol{J} = \frac{1}{2i}\sum_{j=1}^{2}(\psi_j^*\nabla\psi_j - \psi_j\nabla\psi_j^*). \tag{10}$$

This phenomenological dissipation term mimics the viscous term in the Navier-Stokes equation and reduces the

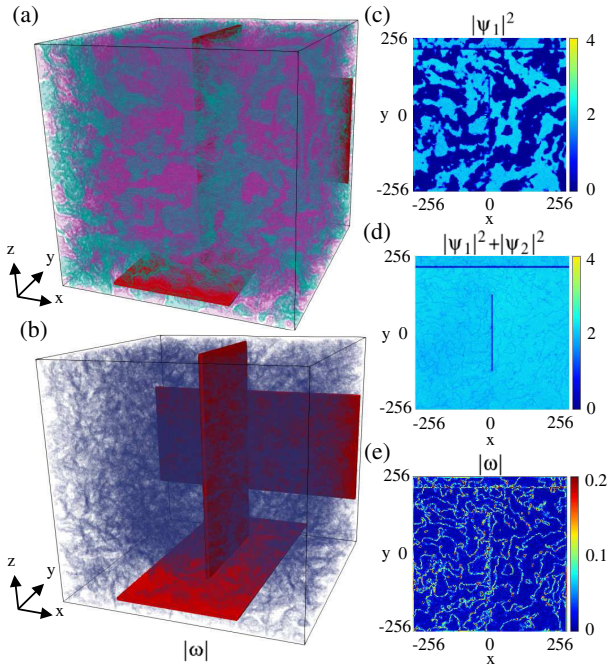

FIG. 1. Snapshots of a fully developed turbulent state at $t = 2000$ for $\tilde{g} \equiv g/(g_{12} - g) = 6.25$ and $M = 0.18$. A two-component BEC is stirred by plate-shaped potentials [red or black in (a) and (b)] to generate a turbulent state. The three plates oscillate in the x, y, and z directions (perpendicular to the surface) from end to end in the box. (a) Isodensity surfaces of $|\psi_1|^2$ (purple or dark gray) and $|\psi_2|^2$ (green or light gray). See the Supplemental Material for a movie of the dynamics [84]. (b) Isodensity surfaces of $|\boldsymbol{\omega}|$. (c), (d), and (e) Cross-sectional views ($z = 0$) of $|\psi_1|^2$, $|\psi_1|^2 + |\psi_2|^2$, and $|\boldsymbol{\omega}|$, respectively.

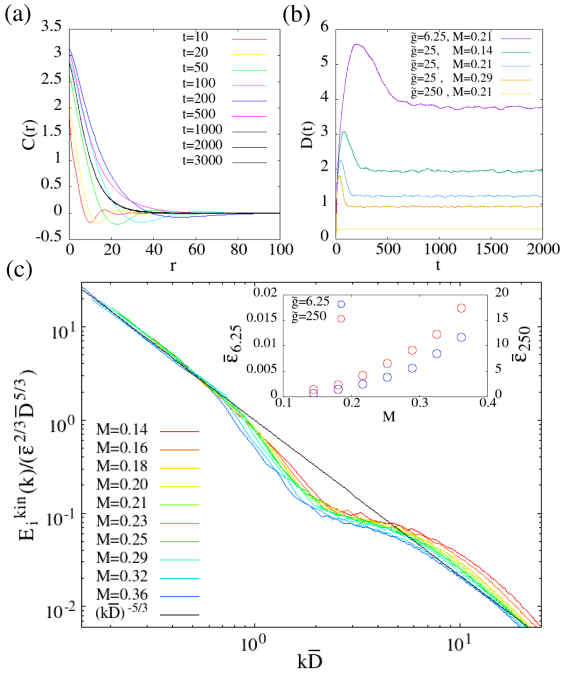

FIG. 2. (a) Time development of the density correlation function $C(r)$ defined in Eq. (11) for $\tilde{g} = 6.25$ and $M = 0.29$. The lines for $t = 1000$, 2000, and 3000 are almost overlapped with each other. (b) Time development of the typical domain size D (full width at half maximum of $C(r)$) for various values of $\tilde{g}$ and M. (c) Incompressible kinetic energy spectra $E_i^{\mathrm{kin}}(k)$ for $\tilde{g} = 6.25$ and various values of M [84], where the time average is taken over two stirring periods. $E_i^{\mathrm{kin}}(k)$ is compensated by $\bar{\epsilon}^{2/3}$ and the length is rescaled by $\bar{D}$, where $\bar{\epsilon}$ and $\bar{D}$ are time-averaged steady values of the energy input rate and the typical domain size, respectively. The straight line represents $E_i^{\mathrm{kin}}(k) = \bar{\epsilon}^{2/3} k^{-5/3}$. The inset shows $\bar{\epsilon}$ as a function of M for $\tilde{g} = 6.25$ and 250.

energy of the system while maintaining the unitarity. The value of γ is selected in such a way that energy dissipation occurs predominantly on a scale below those for the inertial range and the domain size. The larger-scale dynamics are not affected by the details of the dissipation, as long as it occurs on a sufficiently small scale.

Figure 1(a) shows isodensity surfaces of $|\psi_1|^2$ and $|\psi_2|^2$ after the fully developed turbulent state is achieved. The two components are separated and domains are formed in each component because of the immiscible condition $g_{12} > g$. The domain sizes in Fig. 1(a) are typically ~ 10 (note that the length unit is W), and thus the KH scale is expected to be in the region of Eq. (1) [rather than Eq. (3)], which will be investigated later.

Figures 1(c) and 1(d) show cross-sectional views of the densities $|\psi_1|^2$ and $|\psi_1|^2 + |\psi_2|^2$, respectively. Although $|\psi_1|^2$ (or $|\psi_2|^2$) largely varies in space due to the phase separation [Fig. 1(c)], the total density outside of the stirring potentials is almost uniform [Fig. 1(d)]. Density holes arising from quantized vortices are rarely observed [86], since the velocity of the stirring potential is much lower than the sound velocity of the density waves. This situation is different from the quantum turbulence in a single-component system, in which quantized vortices play a central role in the energy cascade. This difference arises because $\oint \boldsymbol{v} \cdot d\boldsymbol{r}$ does not need to be quantized in the two-component system, where the mass-current velocity is $\boldsymbol{v} = \boldsymbol{J}/(|\psi_1|^2 + |\psi_2|^2)$. Figures 1(b) and 1(e) show the distribution of the vorticity $|\boldsymbol{\omega}| = |\nabla \times \boldsymbol{v}|$. There is no singularity in Fig. 1(e); the vorticity is finite and localized around the interfaces of the domains.

The typical size of the domains can be evaluated from the density correlation function,

$$C(r) = \langle d(\boldsymbol{r}') d(\boldsymbol{r}' + \boldsymbol{r}) \rangle, \tag{11}$$

where $d = |\psi_1|^2 - |\psi_2|^2$ is the density-imbalance distribution and $\langle \cdots \rangle$ represents the average over the position $\boldsymbol{r}'$ and the direction of $\boldsymbol{r}$. Figure 2(a) shows the time evolution of $C(r)$. Since the initial wave function has a random distribution, $C(r)$ is initially narrow, which then becomes broader and reaches a steady shape for $t \gtrsim 1000$. We have confirmed that the steady shape of $C(r)$ is independent of the initial state. We define the typical domain size D as the

full width at half maximum of the correlation function $C(r)$. Figure 2(b) shows the time development of D for different values of $\tilde{g}$ and M. The size D first increases because the initial random noise is rapidly dissipated, and a steady size is reached after that. The steady size D decreases with $\tilde{g}$ and M.

The energy input rate per atom is obtained by

$$\epsilon = \frac{\int (|\psi_1|^2 + |\psi_2|^2)\dot{V}_{\rm ext} d\boldsymbol{r}}{\int (|\psi_1|^2 + |\psi_2|^2) d\boldsymbol{r}}, \tag{12}$$

where the time dependence of the potential $V_{\rm ext}$ is given in Eq. (8). The value of ϵ (and also D) fluctuates over time due to the random nature of the turbulence. The sinusoidal motion of the plate-shaped potentials also causes periodic fluctuation. Therefore, we take the temporal average of these quantities, $\bar{\epsilon}$ and $\bar{D}$, over a sufficiently long time after the steady turbulent state is achieved. The inset in Fig. 2(c) shows $\bar{\epsilon}$ as a function of M.

To confirm that the system has reached the Kolmogorov turbulence, we calculate the incompressible kinetic energy spectrum $E_i^{\rm kin}(k)$ of the total mass current (see Supplemental Material for detail [84]), which is shown in Fig. 2(c). Since the Kolmogorov theory predicts $E_i^{\rm kin}(k) \propto \bar{\epsilon}^{2/3} k^{-5/3}$, the plots in Fig. 2(c) are compensated by $\bar{\epsilon}^{2/3}$. The length is also rescaled by the domain size $\bar{D}$ to observe the effect of the domains on the energy spectrum. Figure 2(c) shows that the lines of the energy spectra with different $\bar{\epsilon}$ and $\bar{D}$ collapse into a single universal line with a slope of $\simeq -5/3$ on a scale larger than the domain size ($k\bar{D} \lesssim 1$), which implies that the Kolmogorov energy cascade occurs on this scale. At the scale of $k\bar{D} \sim 1$, the energy cascade is arrested by the domains [11], which results in the deviation from the power law, as shown in Fig. 2(c). This situation is similar to the case of a single-component system, in which the inertial range is terminated at the scale of the mean distance between quantized vortices [16,87].

Now we are ready to investigate the KH scales in a turbulent superfluid in the classical and quantum regimes, as given in Eqs. (1) and (3), respectively. The results are shown in Fig. 3, which are the main results obtained in this study. Figure 3 plots the typical domain size $\bar{D}$ versus the energy input rate $\bar{\epsilon}$ for various values of the Mach number of the stirring potential M and the normalized interaction coefficient $\tilde{g}$. For $\bar{D} \gg W$, the plots obey the $\bar{\epsilon}^{-2/5}$ power law, which agrees with the classical KH scale in Eq. (1). This implies that the two components are well separated and the interfacial tension plays a dominant role to coalesce domains. The fact that the plots with different values of $\tilde{g}$ follow the common line in the present normalization scheme indicates that $\bar{D}$ obeys not only the $\bar{\epsilon}^{-2/5}$ power law but also the $\sigma^{3/5}$ power law in Eq. (1). For $\bar{D} \ll W$, on the other hand, the plots in Fig. 3 obey the $\bar{\epsilon}^{-1/4}$ power law, which agrees with the KH scale in the quantum regime in Eq. (3) and implies that the mechanism that suppresses the disintegration of domains is mainly the quantum kinetic energy arising from the uncertainty principle.

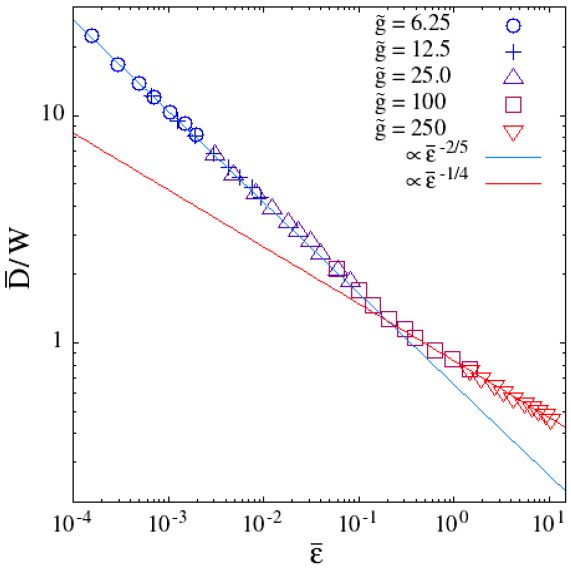

FIG. 3. Typical domain size $\bar{D}$ versus energy input rate $\bar{\epsilon}$ for the steady turbulent state with $\tilde{g} = 6.25$, 12.5, 25, 100, and 250. For each value of $\tilde{g}$, M is varied within an appropriate range (see text). The slopes of the lines are $-2/5$ and $-1/4$ for comparison with Eqs. (1) and (3). The length unit W is explicitly shown in the ordinate for clarity.

In the numerical simulations in Fig. 3, the plot range for each $\tilde{g}$ is restricted, because the domain size $\bar{D}$ is limited by the size of the numerical box, and the energy input rate $\bar{\epsilon}$ is limited by the maximum velocity allowed for the plate-shaped potentials. In the present normalization, the box size is $L = 512\tilde{\xi} = 512/\sqrt{\tilde{g}}$, and hence $\bar{D}$ can be larger for smaller $\tilde{g}$ (left-hand plots in Fig. 3). On the other hand, the Mach number M of the plate-shaped potentials must be smaller than about unity, or the total density would be significantly disturbed and the present picture (domains formed by phase separation) breaks down. In the present unit, the sound velocity is $v_s = \sqrt{2\tilde{g}}$; therefore, we can drive the stirring potential faster for larger $\tilde{g}$. This is the reason why the energy input rate $\bar{\epsilon}$ can be made larger for larger $\tilde{g}$, and the more rightward region can be plotted in Fig. 3. Thus, although $\bar{D}$ and $\bar{\epsilon}$ are restricted to narrow ranges for each value of $\tilde{g}$ in the present numerical simulations, the plots in Fig. 3 can be extended to a wide range, which corroborates the existence of the two power laws in the superfluid KH scale.

Finally, we discuss the possible experimental realization of the present results. A box-shaped trap would be suitable to avoid complexity arising from the inhomogeneous $|\psi_1|^2 + |\psi_2|^2$ distribution in a harmonic trap. The stirring potential can be produced by a far-off-resonance laser beam. Shaking of an optical box can also be used to generate the turbulent state [36]. The typical size of the

domains can be inferred from the imaging data, where slice imaging of a three-dimensional distribution may be required [88]. It is difficult to measure the energy input rate directly; therefore, the support of numerical simulation is necessary, which provides the relation between the motion of the potential and the energy input rate, as in the inset in Fig. 2(c). The interaction g_{12} can be varied using the Feshbach resonance technique.

In conclusion, we have investigated the KH scale of domain sizes in immiscible two-component superfluids in a fully developed turbulent state. We predict that two regions of the KH scale exist with different power laws, which reflect the quantum properties of the system. Numerical simulations of the coupled GP equations were performed, and the typical domain size $\bar{D}$ was confirmed to obey the power laws with respect to the energy input rate $\bar{\epsilon}$. The power changes from $-2/5$ to $-1/4$ with increasing $\bar{\epsilon}$, and the crossover between these classical and quantum KH scales is located at the region where $\bar{D}$ is comparable to the length scale W in Eq. (5). For a two-dimensional system, the enstrophy cascade may be observed, which will be studied elsewhere.

Acknowledgments—This work was supported by JSPS KAKENHI Grants No. JP20K03804 and No. JP23K03276.

[1] A. N. Kolmogorov, On the breakage of drops in a turbulent flow, Dokl. Akad. Nauk SSSR **66**, 825 (1949).
[2] J. O. Hinze, Fundamentals of the hydrodynamic mechanism of splitting in dispersion process, AIChE J. **1**, 289 (1955).
[3] See, e. g., and U. Frisch, *Turbulence: The Legacy of A. N. Kolmogorov* (Cambridge University Press, Cambridge, England, 1995).
[4] P. H. Clay, The mechanism of emulsion formation in turbulent flow, Proc. R. Acad. Sci. (Amsterdam) **43**, 852 (1940).
[5] R. Shinnar, On the behaviour of liquid dispersions in mixing vessels, J. Fluid Mech. **10**, 259 (1961).
[6] C. A. Sleicher, Maximum stable drop size in turbulent flow, AIChE J. **8**, 471 (1964).
[7] K. Arai, M. Konno, Y. Matunaga, and S. Saito, Effect of dispersed-phase viscosity on the stable drop size for breakup in turbulent flow, J. Chem. Eng. Jpn. **10**, 325 (1977).
[8] G. B. Deane and M. D. Stokes, Scale dependence of bubble creation mechanisms in breaking waves, Nature (London) **418**, 839 (2002).
[9] P. Perlekar, L. Biferale, M. Sbragaglia, S. Srivastava, and F. Toschi, Droplet size distribution in homogeneous isotropic turbulence, Phys. Fluids **24**, 065101 (2012).
[10] R. Skartlien, E. Sollum, and H. Schumann, Droplet size distributions in turbulent emulsions: Breakup criteria and surfactant effects from direct numerical simulations, J. Chem. Phys. **139**, 174901 (2013).
[11] P. Perlekar, R. Benzi, H. J. H. Clercx, D. R. Nelson, and F. Toschi, Spinodal decomposition in homogeneous and isotropic turbulence, Phys. Rev. Lett. **112**, 014502 (2014).
[12] X. Fan, P. H. Diamond, L. Chacón, and H. Li, Cascades and spectra of a turbulent spinodal decomposition in two-dimensional symmetric binary liquid mixtures, Phys. Rev. Fluids **1**, 054403 (2016).
[13] P. Perlekar, N. Pal, and R. Pandit, Two-dimensional turbulence in symmetric binary-fluid mixtures: Coarsening arrest by the inverse cascade, Sci. Rep. **7**, 44589 (2017).
[14] M. E. Rosti, Z. Ge, S. S. Jain, M. S. Dodd, and L. Brandt, Droplets in homogeneous shear turbulence, J. Fluid Mech. **876**, 962 (2019).
[15] M. Crialesi-Esposito, M. E. Rosti, S. Chibbaro, and L. Brandt, Modulation of homogeneous and isotropic turbulence in emulsions, J. Fluid Mech. **940**, A19 (2022).
[16] C. Nore, M. Abid, and M. E. Brachet, Kolmogorov turbulence in low-temperature superflows, Phys. Rev. Lett. **78**, 3896 (1997).
[17] C. Nore, M. Abid, and M. E. Brachet, Decaying Kolmogorov turbulence in a model of superflow, Phys. Fluids **9**, 2644 (1997).
[18] S. R. Stalp, L. Skrbek, and R. J. Donnelly, Decay of grid turbulence in a finite channel, Phys. Rev. Lett. **82**, 4831 (1999).
[19] T. Araki, M. Tsubota, and S. K. Nemirovskii, Energy spectrum of superfluid turbulence with no normal-fluid component, Phys. Rev. Lett. **89**, 145301 (2002).
[20] M. Kobayashi and M. Tsubota, Kolmogorov spectrum of superfluid turbulence: numerical analysis of the Gross-Pitaevskii equation with a small-scale dissipation, Phys. Rev. Lett. **94**, 065302 (2005).
[21] M. Kobayashi and M. Tsubota, Kolmogorov spectrum of quantum turbulence, J. Phys. Soc. Jpn. **74**, 3248 (2005).
[22] N. G. Parker and C. S. Adams, Emergence and decay of turbulence in stirred atomic Bose-Einstein condensates, Phys. Rev. Lett. **95**, 145301 (2005).
[23] N. Sasa, T. Kano, M. Machida, V. S. L'vov, O. Rudenko, and M. Tsubota, Energy spectra of quantum turbulence: Large-scale simulation and modeling, Phys. Rev. B **84**, 054525 (2011).
[24] A. W. Baggaley, J. Laurie, and C. F. Barenghi, Vortex-density fluctuations, energy spectra, and vortical regions in superfluid turbulence, Phys. Rev. Lett. **109**, 205304 (2012).
[25] P. C. di Leoni, P. D. Mininni, and M. E. Brachet, Dual cascade and dissipation mechanisms in helical quantum turbulence, Phys. Rev. A **95**, 053636 (2017).
[26] P. C. di Leoni, P. D. Mininni, and M. E. Brachet, Finite-temperature effects in helical quantum turbulence, Phys. Rev. A **97**, 043629 (2018).
[27] V. Shukla, P. D. Mininni, G. Krstulovic, P. C. di Leoni, and M. E. Brachet, Quantitative estimation of effective viscosity in quantum turbulence, Phys. Rev. A **99**, 043605 (2019).
[28] N. P. Müller, J. I. Polanco, and G. Krstulovic, Intermittency of velocity circulation in quantum turbulence, Phys. Rev. X **11**, 011053 (2021).
[29] J. I. Polanco, N. P. Müller, and G. Krstulovic, Vortex clustering, polarisation and circulation intermittency in classical and quantum turbulence, Nat. Commun. **12**, 7090 (2021).
[30] M. Kobayashi, P. Parnaudeau, F. Luddens, C. Lothodé, L. Danaila, M. Brachet, and I. Danaila, Quantum turbulence

simulations using the Gross-Pitaevskii equation: High-performance computing and new numerical benchmarks, Comput. Phys. Commun. **258**, 107579 (2021).
[31] J. A. Estrada, M. E. Brachet, and P. D. Mininni, Turbulence in rotating Bose-Einstein condensates, Phys. Rev. A **105**, 063321 (2022).
[32] E. A. L. Henn, J. A. Seman, G. Roati, K. M. F. Magalhães, and V. S. Bagnato, Emergence of turbulence in an oscillating Bose-Einstein condensate, Phys. Rev. Lett. **103**, 045301 (2009).
[33] T. W. Neely, A. S. Bradley, E. C. Samson, S. J. Rooney, E. M. Wright, K. J. H. Law, R. Carretero-González, P. G. Kevrekidis, M. J. Davis, and B. P. Anderson, Characteristics of two-dimensional quantum turbulence in a compressible superfluid, Phys. Rev. Lett. **111**, 235301 (2013).
[34] W. J. Kwon, G. Moon, J.-Y. Choi, S. W. Seo, and Y.-I. Shin, Relaxation of superfluid turbulence in highly oblate Bose-Einstein condensates, Phys. Rev. A **90**, 063627 (2014).
[35] K. J. Thompson, G. G. Bagnato, G. D. Telles, M. A. Caracanhas, F. E. A. dos Santos, and V. S. Bagnato, Evidence of power law behavior in the momentum distribution of a turbulent trapped Bose-Einstein condensate, Laser Phys. Lett. **11**, 015501 (2014).
[36] N. Navon, A. L. Gaunt, R. P. Smith, and Z. Hadzibabic, Emergence of a turbulent cascade in a quantum gas, Nature (London) **539**, 72 (2016).
[37] S. P. Johnstone, A. J. Groszek, P. T. Starkey, C. J. Billington, T. P. Simula, and K. Helmerson, Evolution of large-scale flow from turbulence in a two-dimensional superfluid, Science **364**, 1267 (2019).
[38] N. Navon, C. Eigen, J. Zhang, R. Lopes, A. L. Gaunt, K. Fujimoto, M. Tsubota, R. P. Smith, and Z. Hadzibabic, Synthetic dissipation and cascade fluxes in a turbulent quantum gas, Science **366**, 382 (2019).
[39] M. Gałka, P. Christodoulou, M. Gazo, A. Karailiev, N. Dogra, J. Schmitt, and Z. Hadzibabic, Emergence of isotropy and dynamic scaling in 2D wave turbulence in a homogeneous Bose gas, Phys. Rev. Lett. **129**, 190402 (2022).
[40] A. D. García-Orozco, L. Madeira, M. A. Moreno-Armijos, A. R. Fritsch, P. E. S. Tavares, P. C. M. Castilho, A. Cidrim, G. Roati, and V. S. Bagnato, Universal dynamics of a turbulent superfluid Bose gas, Phys. Rev. A **106**, 023314 (2022).
[41] S. Nazarenko and M. Onorato, Freely decaying turbulence and Bose-Einstein Condensation in Gross-Pitaevski model, J. Low Temp. Phys. **146**, 31 (2007).
[42] T.-L. Horng, C.-H. Hsueh, S.-W. Su, Y.-M. Kao, and S.-C. Gou, Two-dimensional quantum turbulence in a nonuniform Bose-Einstein condensate, Phys. Rev. A **80**, 023618 (2009).
[43] R. Numasato, M. Tsubota, and V. S. L'vov, Direct energy cascade in two-dimensional compressible quantum turbulence, Phys. Rev. A **81**, 063630 (2010).
[44] A. S. Bradley and B. P. Anderson, Energy spectra of vortex distributions in two-dimensional quantum turbulence, Phys. Rev. X **2**, 041001 (2012).
[45] M. T. Reeves, T. P. Billam, B. P. Anderson, and A. S. Bradley, Inverse energy cascade in forced two-dimensional quantum turbulence, Phys. Rev. Lett. **110**, 104501 (2013).
[46] A. W. Baggaley and C. F. Barenghi, Decay of homogeneous two-dimensional quantum turbulence, Phys. Rev. A **97**, 033601 (2018).
[47] N. P. Müller, M.-E. Brachet, A. Alexakis, and P. D. Mininni, Abrupt transition between three-dimensional and two-dimensional quantum turbulence, Phys. Rev. Lett. **124**, 134501 (2020).
[48] N. P. Müller and G. Krstulovic, Exploring the equivalence between two-dimensional classical and quantum turbulence through velocity circulation statistics, Phys. Rev. Lett. **132**, 094002 (2024).
[49] T. Bland, G. W. Stagg, L. Galantucci, A. W. Baggaley, and N. G. Parker, Quantum ferrofluid turbulence, Phys. Rev. Lett. **121**, 174501 (2018).
[50] G. W. Stagg, N. G. Parker, and C. F. Barenghi, Superfluid boundary layer, Phys. Rev. Lett. **118**, 135301 (2017).
[51] N. G. Berloff and C. Yin, Turbulence and coherent structures in two-component Bose condensates, J. Low Temp. Phys. **145**, 187 (2006).
[52] H. Takeuchi, S. Ishino, and M. Tsubota, Binary quantum turbulence arising from countersuperflow instability in two-component Bose-Einstein condensates, Phys. Rev. Lett. **105**, 205301 (2010).
[53] K. Fujimoto and M. Tsubota, Counterflow instability and turbulence in a spin-1 spinor Bose-Einstein condensate, Phys. Rev. A **85**, 033642 (2012).
[54] K. Fujimoto and M. Tsubota, Spin turbulence in a trapped spin-1 spinor Bose-Einstein condensate, Phys. Rev. A **85**, 053641 (2012).
[55] K. Fujimoto and M. Tsubota, Spin turbulence with small spin magnitude in spin-1 spinor Bose-Einstein condensates, Phys. Rev. A **88**, 063628 (2013).
[56] K. Fujimoto and M. Tsubota, Spin-superflow turbulence in spin-1 ferromagnetic spinor Bose-Einstein condensates, Phys. Rev. A **90**, 013629 (2014).
[57] K. Fujimoto and M. Tsubota, Direct and inverse cascades of spin-wave turbulence in spin-1 ferromagnetic spinor Bose-Einstein condensates, Phys. Rev. A **93**, 033620 (2016).
[58] M. Tsubota, Y. Aoki, and K. Fujimoto, Spin-glass-like behavior in the spin turbulence of spinor Bose-Einstein condensates, Phys. Rev. A **88**, 061601(R) (2013).
[59] B. Villaseñor, R. Zamora-Zamora, D. Bernal, and V. Romero-Rochín, Quantum turbulence by vortex stirring in a spinor Bose-Einstein condensate, Phys. Rev. A **89**, 033611 (2014).
[60] D. Kobyakov, A. Bezett, E. Lundh, M. Marklund, and V. Bychkov, Turbulence in binary Bose-Einstein condensates generated by highly nonlinear Rayleigh-Taylor and Kelvin-Helmholtz instabilities, Phys. Rev. A **89**, 013631 (2014).
[61] S. Kang, S. W. Seo, J. H. Kim, and Y. Shin, Emergence and scaling of spin turbulence in quenched antiferromagnetic spinor Bose-Einstein condensates, Phys. Rev. A **95**, 053638 (2017).
[62] T. Mithun, K. Kasamatsu, B. Dey, and P. G. Kevrekidis, Decay of two-dimensional quantum turbulence in binary Bose-Einstein condensates, Phys. Rev. A **103**, 023301 (2021).
[63] S. Das, K. Mukherjee, and S. Majumder, Vortex formation and quantum turbulence with rotating paddle potentials in a

two-dimensional binary Bose-Einstein condensate, Phys. Rev. A **106**, 023306 (2022).
[64] A. N. da Silva, R. K. Kumar, A. S. Bradley, and L. Tomio, Vortex generation in stirred binary Bose-Einstein condensates, Phys. Rev. A **107**, 033314 (2023).
[65] M. Karl, B. Nowak, and T. Gasenzer, Tuning universality far from equilibrium, Sci. Rep. **3**, 2394 (2013).
[66] M. Karl, B. Nowak, and T. Gasenzer, Universal scaling at nonthermal fixed points of a two-component Bose gas, Phys. Rev. A **88**, 063615 (2013).
[67] K. Kudo and Y. Kawaguchi, Magnetic domain growth in a ferromagnetic Bose-Einstein condensate: Effects of current, Phys. Rev. A **88**, 013630 (2013).
[68] K. Kudo and Y. Kawaguchi, Coarsening dynamics driven by vortex-antivortex annihilation in ferromagnetic Bose-Einstein condensates, Phys. Rev. A **91**, 053609 (2015).
[69] J. Hofmann, S. S. Natu, and S. Das Sarma, Coarsening dynamics of binary Bose condensates, Phys. Rev. Lett. **113**, 095702 (2014).
[70] S. De, D. L. Campbell, R. M. Price, A. Putra, B. M. Anderson, and I. B. Spielman, Quenched binary Bose-Einstein condensates: Spin-domain formation and coarsening, Phys. Rev. A **89**, 033631 (2014).
[71] E. Nicklas, M. Karl, M. Höfer, A. Johnson, W. Muessel, H. Strobel, J. Tomkovič, T. Gasenzer, and M. K. Oberthaler, Observation of scaling in the dynamics of a strongly quenched quantum gas, Phys. Rev. Lett. **115**, 245301 (2015).
[72] L. A. Williamson and P. B. Blakie, Universal coarsening dynamics of a quenched ferromagnetic spin-1 condensate, Phys. Rev. Lett. **116**, 025301 (2016).
[73] L. A. Williamson and P. B. Blakie, Coarsening and thermalization properties of a quenched ferromagnetic spin-1 condensate, Phys. Rev. A **94**, 023608 (2016).
[74] L. A. Williamson and P. B. Blakie, Coarsening dynamics of an isotropic ferromagnetic superfluid, Phys. Rev. Lett. **119**, 255301 (2017).
[75] A. Bourges and P. B. Blakie, Different growth rates for spin and superfluid order in a quenched spinor condensate, Phys. Rev. A **95**, 023616 (2017).
[76] M. Prüfer, P. Kunkel, H. Strobel, S. Lannig, D. Linnemann, C.-M. Schmied, J. Berges, T. Gasenzer, and M. K. Oberthaler, Observation of universal dynamics in a spinor Bose gas far from equilibrium, Nature (London) **563**, 217 (2018).
[77] K. Fujimoto, R. Hamazaki, and M. Ueda, Unconventional universality class of one-dimensional isolated coarsening dynamics in a spinor Bose gas, Phys. Rev. Lett. **120**, 073002 (2018).
[78] H. Takeuchi, Domain-area distribution anomaly in segregating multicomponent superfluids, Phys. Rev. A **97**, 013617 (2018).
[79] L. M. Symes, D. Baillie, and P. B. Blakie, Dynamics of a quenched spin-1 antiferromagnetic condensate in a harmonic trap, Phys. Rev. A **98**, 063618 (2018).
[80] P. Ao and S. T. Chui, Binary Bose-Einstein condensate mixtures in weakly and strongly segregated phases, Phys. Rev. A **58**, 4836 (1998).
[81] R. A. Barankov, Boundary of two mixed Bose-Einstein condensates, Phys. Rev. A **66**, 013612 (2002).
[82] B. V. Schaeybroeck, Interface tension of Bose-Einstein condensates, Phys. Rev. A **78**, 023624 (2008); Phys. Rev. A **80**, 065601 (2009).
[83] See, e. g., C. J. Pethick, and H. Smith, *Bose-Einstein Condensation in Dilute Gases*, 2nd ed. (Cambridge University Press, Cambridge, England, 2008), Chap. 12.
[84] See Supplemental Material at http://link.aps.org/supplemental/10.1103/PhysRevLett.133.256001, which includes Refs. [16,20,21], for additional information about the energy dissipation, nondimensionalization, kinetic energy spectra, and two-thirds law. Supplemental Material also includes a movie showing the dynamics of the system.
[85] W. H. Press, S. A. Teukolsky, W. T. Vetterling, and B. P. Flannery, *Numerical Recipes*, 3rd ed. (Cambridge University Press, Cambridge, England, 2007).
[86] The quantized vortices in each component are pushed into regions occupied by the other component. See, e.g., K. Kasamatsu, M. Tsubota, and M. Ueda, Vortex phase diagram in rotating two-component Bose-Einstein condensates, Phys. Rev. Lett. **91**, 150406 (2003).
[87] V. S. L'vov, S. V. Nazarenko, and O. Rudenko, Bottleneck crossover between classical and quantum superfluid turbulence, Phys. Rev. B **76**, 024520 (2007).
[88] M. R. Andrews, C. G. Townsend, H.-J. Miesner, D. S. Durfee, D. M. Kurn, and W. Ketterle, Observation of interference between two Bose condensates, Science **275**, 637 (1997).